

**Inhibited Inelastic Scattering of Incoherent Excitons for Near-Band Edge Excitations**D. Anders<sup>1</sup>, F. Dobener<sup>1</sup>, F. Schäfer<sup>1</sup>, S. Chatterjee<sup>1</sup>, and M. Stein<sup>1\*</sup>*Institute of Experimental Physics I and Center for Materials Research (LaMa), Justus-Liebig-University Giessen, Heinrich-Buff-Ring 16, D-35392 Giessen, Germany*

(Received 11 August 2023; accepted 12 February 2024; published 5 March 2024)

A multiple pump-terahertz probe experiment enables the clear distinction between elastic and inelastic scattering of excitons with a free electron-hole plasma in (Ga,In)As multi-quantum wells. Low plasma energies dictate the prevalence of elastic scattering by inhibiting inelastic processes due to the absence of final states for quasiparticles. Yet, an increased plasma energy results in a progressive destruction of excitons. Notably, despite plasma energy variations, the interaction strength between excitons and the electron-hole plasma remains unaltered.

DOI: [10.1103/PhysRevLett.132.106901](https://doi.org/10.1103/PhysRevLett.132.106901)

Scattering is a fundamental concept native to many branches of physics, spanning astrophysics, classical mechanics, quantum mechanics, nuclear physics, and solid-state physics. The latter commonly describes complex interacting many-body systems where scattering processes naturally play a pivotal role. To simplify the mathematical description of these systems, the concept of quasiparticles emerges, treating these collective excitations as new particles with unique properties instead of individual interactions between a vast number of (elementary) particles [1,2]. As such they exhibit a dispersion relation and are capable of scattering with each other, exchanging energy and momentum.

The interaction of quasiparticles plays a crucial role in determining the performance of many semiconductor-based devices, including lasers, solar cells, and transistors [3–6]. Moreover, scattering processes are fundamental in investigating phenomena like Bose-Einstein condensates of excitons, i.e., bound electron hole pairs [7], superconductivity [8], dynamical Bloch oscillations [9], or Floquet-Bloch bands [10]. Accordingly, extensive research has been dedicated to investigate scattering processes between quasiparticles, particularly excitons and electrons in semiconductors [11–19].

The coherent lifetime and optical linewidths of excitons have been widely utilized to study these processes, both of which are significantly affected by scattering. Four-wave-mixing spectroscopy (FWM) can be employed to directly quantify the dephasing of exciton polarizations in the presence of either an electron-hole plasma or incoherent excitons [11,12,20–23]. Furthermore, the broadening of exciton transitions offer insights into electron-exciton scattering dynamics, as dephasing times inversely correlate with homogeneous linewidths [12,21]. This is effectively utilized in time-resolved photoluminescence (TRPL) spectroscopy and optical transmission experiments [24–29]. Again, additional excitation pulses can tailor the desired

scattering environment [23,26]. However, such experimental investigations only provide information on the rate at which scattering events occur, yet, they are unable to distinguish between inelastic and elastic scattering, i.e., they cannot identify if energy is dissipated or if both the energy and the translational momentum are rigorously conserved. This requires an additional measure, namely, quantitative information on the size of the exciton population. These data are hard to access by purely optical means [30] while terahertz (THz) spectroscopy more conveniently provides a measure for the exciton population [31,32].

THz pulses probe transitions between excitonic energy levels, irrespective of the exciton's center-of-mass momentum [32]. Specifically, the transition between the exciton ground state and an excited state, such as the  $1s$  to  $2p$  transition, is directly proportional to the population of the  $1s$  exciton ground state [31]. Therefore, THz probe spectroscopy becomes an ideal tool to detect inelastic scattering processes that result in the destruction of  $1s$  exciton populations [33].

In this Letter, we elucidate the robustness of bound quasiparticles, here specifically incoherent excitons, to ionization due to energy transfer by inelastic scattering. To explore this phenomenon, we study the scattering of a pre-injected incoherent exciton population with a free electron-hole plasma by varying the excess energy of the plasma and its charge-carrier density. By analyzing the exciton-population decay-dynamics following the injection of an electron-hole plasma, we determine the inelastic scattering parameter for different excess energies of the injected plasma. Simultaneously, the presence of the electron-hole plasma manifests through spectral broadening of the intraexcitonic  $1s$ - $2p$  absorption line, allowing us to directly monitor the total scattering.

We employ a multiple optical pump—terahertz probe setup featuring two independently tunable optical pulses to

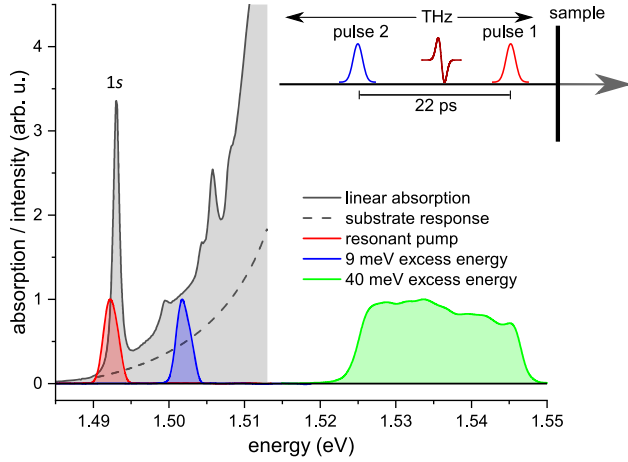


FIG. 1. Absorption (gray) of the (Ga,In)As quantum wells. The absorption of the GaAs substrate is shown as a dashed line. The first optical pulse (red) resonantly excites a  $1s$  exciton population. The blue and green pulses correspond to the second optical pulse with excess energies of 9 and 40 meV with respect to the  $1s$  exciton resonance, respectively. The inset illustrates the pulse sequence of the experiment.

study a high-quality multiple quantum well structure. Details of the sample structure as well as the experimental setup are available in the Supplemental Material at Ref. [34]. Figure 1 displays the linear absorption spectrum of the sample, revealing a pronounced  $1s$  exciton resonance at 1.493 eV. The first pulse resonantly excites the sample at this exciton transition; its spectrum is shown in red. Subsequently, this excitation turns into an incoherent quasi-steady-state exciton population. The second pulse injects the scattering partners 22 ps after the initial pulse. Its spectral position determines the excess energy of the additional electron-hole plasma. The representative excitation spectra corresponding to 9 and 40 meV excess energy relative to the  $1s$  exciton resonance are given in blue and green, respectively. The response of the quasiparticles at a given time delay between the optical excitation pulses and the THz pulse is analyzed by sampling the ps-long THz pulse in the time domain. Changing the time delay of the THz pulse yields the time-dependent quasiparticle response. This is illustrated in the inset of Fig. 1.

A phenomenological Drude-Lorentz model describes the pump-induced changes of the frequency-dependent dielectric function  $\Delta\epsilon(\omega) = \Delta\epsilon_1(\omega) + i\Delta\epsilon_2(\omega)$  which is monitored by the THz response. Its quantitative analysis disentangles the individual quasiparticle dynamics [38]. The Drude response is typical for a free electron-hole plasma [35], while a  $1s$  exciton population manifests itself in an intraexcitonic transition described by a Lorentzian oscillator [32]. The simultaneous fit to both, the real and the imaginary part of  $\Delta\epsilon(\omega)$  yields robust results for the homogeneous linewidth  $\Delta_{\text{hom}}$  and the exciton sheet-density  $n_x$ . Further details are provided in the Supplemental Material [34].

Figure 2(a) shows contour plots of the THz-absorption for 9 (left) and 40 meV (right) excess energy of the respective second excitation pulses. The charge-carrier density of the additionally injected carriers is kept comparable at  $4.6 \times 10^9$  and  $4.8 \times 10^9 \text{ cm}^{-2}$  for 9 and 40 meV surplus energy, respectively. The pronounced absorption peak at 1.36 THz observed at early times indicates that the first optical pulse creates a pure  $1s$  exciton population. After a 22 ps delay, the second pulse interacts with the sample. The data distinctly reveal varying THz absorption depending on the excess energy of the second pulse. For 9 meV excess energy, the intraexcitonic transition at 1.36 THz broadens significantly and slightly shifts towards lower frequencies. Similarly, with 40 meV excess energy, the intraexcitonic transition also broadens shortly after the second pulse. In this case, however, the intraexcitonic oscillator strength additionally decreases and simultaneously gives rise to a Drude-like plasma response at frequencies below 0.5 THz [35]. Thus, the breakup of a  $1s$  exciton population into a free electron-hole plasma due to inelastic scattering of excitons with a hot electron-hole plasma is caught red handed. This is vividly illustrated in Fig. 2(b), which shows the intraexcitonic linewidth against excitation density for both excess energies, and the intraexcitonic oscillator strength relative to its value prior to the injection of the electron-hole plasma by the second pulse. It is apparent that both excitation conditions result in a comparable broadening of the intraexcitonic resonance, which increases with charge carrier density. However, the oscillator strength notably decreases with rising density for the 40 meV excess energy excitation, dropping to a mere one-third of its original strength at the highest excitation density. In contrast, for the low excess energy excitation, despite a similar broadening of the intraexcitonic resonance, there is only a marginal reduction in oscillator strength, partly attributable to radiative recombination processes. The distinct difference in oscillator strength between the two excess energies unequivocally stems from the significantly more frequent occurrence of inelastic scattering processes at 40 meV excess energy.

Elastic scattering on the one hand exchanges momentum and kinetic energy between the two scattering partners. Here, excitons and electrons persist, however, now featuring modified center-of-mass momenta. Consequently, elastic scattering processes only change the phase of the  $1s$  excitons and do not affect the oscillator strength associated with the intraexciton transitions [39]. On the other hand, inelastic scattering dissipates parts of the kinetic energy into another form of energy. In this case, the electron and exciton exchange enough energy to excite the exciton into a higher-energy (bound) state or even overcome its binding energy and ionize the exciton. Consequently, this either results in one electron and one exciton in a higher-energy excited state or two free electrons and a hole due to inelastic scattering.

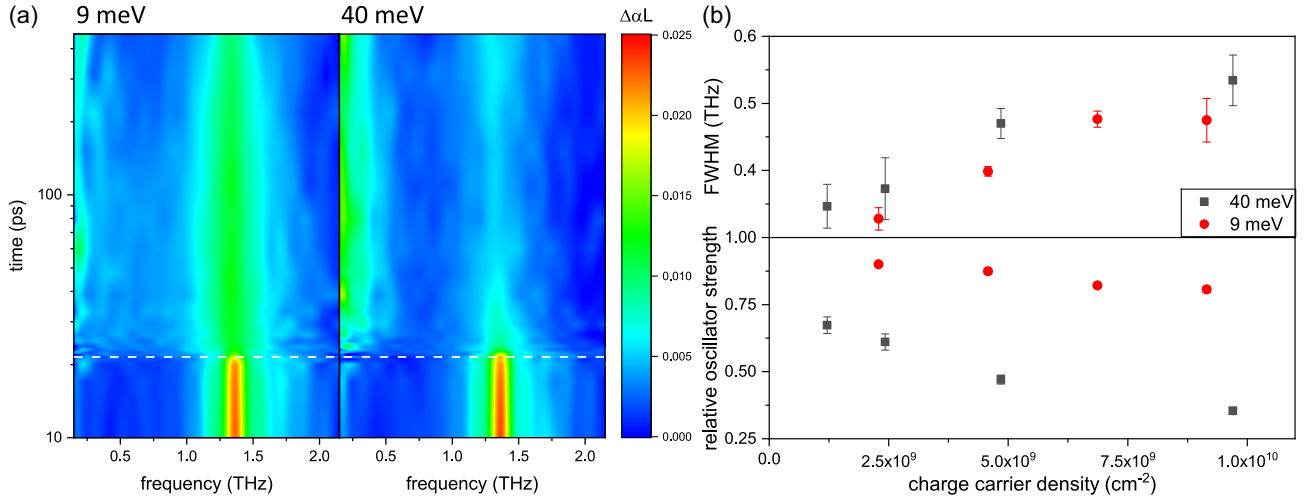


FIG. 2. (a) THz absorption for 9 (left) and 40 meV (right) excess energy of the electron-hole plasma with charge-carrier densities of  $4.6 \times 10^9$  and  $4.8 \times 10^9$   $\text{cm}^{-2}$  respectively. The time of arrival of the second pulse on the sample is marked by the dashed white line. (b) FWHM (top) and oscillator strength (bottom) of the  $1s - 2p$  transition. The relative oscillator strength is derived by dividing the oscillator strength after the arrival of the second pulse by the oscillator strength before the second pulse.

To quantify these inelastic scattering processes, we examine the exciton component  $n_x$  of the Drude-Lorentz model for each time step. Fitting an exponential function to the decreasing exciton fraction after the arrival of the second optical pulse yields the decay time  $\tau_1$  of the exciton population caused solely by the inelastic scattering with the electron-hole plasma. The inelastic scattering induces a homogeneous broadening of the  $1s$  state according to  $\Delta_{\text{hom}} = 2/\tau_1$  [11].

All scattering processes contribute to the broadening of the intraexcitonic transition while only inelastic scattering processes contribute to the destruction of the exciton population. In analogy to optical transmission, FWM or TRPL experiments, we correlate the change of the intraexcitonic linewidth with the total scattering rate [11,40–42]. The excitation-induced intraexcitonic line broadening  $\Delta_{\text{intra}}$  is determined by comparing the intraexcitonic linewidth before  $[\Gamma_{\text{hom}}(0)]$  and after the second optical pulse interacts with the sample  $[\Gamma_{\text{hom}}(n)]$ :

$$\Delta_{\text{intra}} = \Gamma_{\text{hom}}(n) - \Gamma_{\text{hom}}(0). \quad (1)$$

Since the intraexcitonic linewidth of the  $1s-2p$  transition is influenced by scattering processes in both the  $1s$  and  $2p$  states, we assume equal contributions from both states. Consequently, the broadening of the  $1s$  exciton state ( $\Delta_{\text{hom}}$ ) can be expressed as  $\Delta_{\text{hom}} = \Delta_{\text{intra}}/\sqrt{2}$ . To enhance accuracy, we average the linewidth of the  $1s - 2p$  transition from 14 to 17 ps after the initial resonant excitation, i.e., 5–8 ps before the second pulse and from 27–33 ps which is 5–11 ps after the second pulse.

In Fig. 3(a) the excitation-induced broadening of the  $1s$  exciton state  $\Delta_{\text{hom}}$  is plotted against the charge-carrier density induced by the second pulse. This figure also

illustrates the broadening of the  $1s$  exciton state caused by inelastic scattering for an excess energy of the optically induced electron-hole plasma of 40 meV. In the low-density regime, the broadening of the homogeneous linewidth of the  $1s$  state exhibits a linear density dependence [43]. Therefore, we fit the experimental data in Fig. 3(a) using

$$\Delta_{\text{hom}} = \gamma a_B^2 E_B n, \quad (2)$$

where  $a_B$  is the exciton Bohr radius,  $E_B$  the exciton binding energy,  $n$  the charge-carrier density, and  $\gamma$  is a dimensionless parameter representing the interaction strength of excitons with the free electron-hole plasma. The exciton binding energy in quantum well systems is well approximated by multiplying the resonance energy of the intraexcitonic  $1s-2p$  transition by 9/8 [44]. For our case, this yields an exciton binding energy of  $E_B = 6.33$  meV. Since the product of  $E_B \cdot a_B$  is constant for a material system [45], we can use the exciton binding energy and the Bohr radius of a very similar quantum well structure [46] to derive an exciton Bohr radius of 11 nm for our sample. This allows us to determine the scattering parameter  $\gamma$  from the slope  $m$  of the fits in Fig. 3(a) according to

$$\gamma = \frac{m}{a_B^2 E_B}. \quad (3)$$

The elastic contribution ( $\gamma_{\text{el}}$ ) to the total scattering parameter is then deduced by subtracting the inelastic scattering parameter from the total scattering parameter.

Table I shows the extracted total scattering parameters as well as their elastic and inelastic contributions for both excess energies. The total scattering parameters  $\gamma_{\text{tot},9 \text{ meV}} = 8.8$  and  $\gamma_{\text{tot},40 \text{ meV}} = 9.32$  are similar. Both overlap within the margins of error of the scattering parameters determined

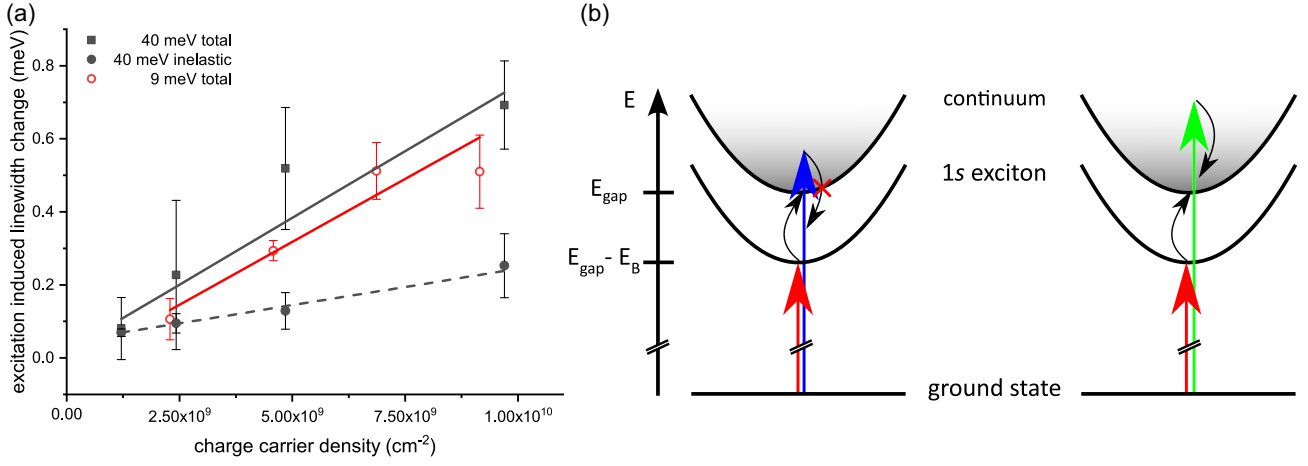


FIG. 3. (a) Change of the  $1s$  exciton linewidth induced by the additional charge carriers with an excess energy of 40 meV (grey) and 9 meV (red), respectively. The scattering parameters are derived from the linear fits to the density-dependent  $1s$  exciton line broadening. (b) Schematic drawing of the inelastic scattering processes for 9 (left) and 40 meV (right) excess energy. The short black arrows indicate the energy transfer between the  $1s$  excitons and the free charge carriers.

in Ref. [11] for a 12 nm GaAs single quantum well and about a factor of 2 larger than the one found for similar (Ga, In)As quantum well structures [22]. For 9 meV excess energy, the inelastic scattering is negligible as evident by the minimal change in exciton density  $n_x$ . In contrast, the inelastic scattering parameter amounts to 2.54 for 40 meV excess energy which results in an elastic scattering parameter of 6.78.

Interestingly, virtually no inelastic scattering is observed at 9 meV excess energy, regardless of the carrier density injected by the second pulse. Notably, charge carriers injected with a surplus energy of 9 meV above the  $1s$  exciton resonance should have enough excess energy to overcome the 6.33 meV binding energy and, thus, dissociate excitons in scattering events. To explain the lack of inelastic scattering, we have to revisit the linear absorption spectrum given as gray-shaded area in Fig. 1 and consider Fermi's golden rule. The latter states in simple terms that scattering processes require both occupied initial states and unoccupied final states in addition to an interaction strength. From Fig. 1 it is apparent that there are no final states between the  $1s$  exciton resonance and the conduction band edge that electrons can occupy after an inelastic scattering event with an exciton, i.e., an energy exchange of

at least 5.6 meV necessary to bring it into an excited state. Consequently, inelastic scattering of excitons with charge carriers close to the band edge is strongly suppressed as there are no states available for electrons to occupy after the scattering event. This phenomenon is visually depicted in Fig. 3(b). Here, the energy transfer linked to an inelastic scattering process involving a  $1s$  exciton would propel the excited electron-hole plasma (indicated by the blue arrow), carrying an excess energy of 9 meV, into a restricted energy region within the semiconductor structure. Only for higher excitation energies, represented by the green arrow in Fig. 3(b), the electron-hole plasma finds states in the continuum that can be occupied after the energy transfer required for an inelastic scattering process. However, the energy of an electron-hole plasma is only linked to the optical pulse-width during excitation. The electron-hole plasma rapidly thermalizes following excitation on a picosecond timescale and adopts a Fermi-Dirac-like energy distribution. The thermalization leads to a broader energy distribution among the charge carriers, with their average energy matching the initial excess energy. Consequently, a small proportion of charge carriers gain enough energy to dissociate excitons even for 9 meV excess energy. This is also reflected in our data in Fig. 2(a). The excitation by the second optical pulse with 9 meV excess energy invokes a moderate yet discernible plasma response. This indicates the presence of a small fraction of an unbound electron-hole plasma. These spectra thus provide clear evidence of inelastic scattering processes, even if they are too infrequent for precise quantification via a decaying exciton population.

TABLE I. Scattering parameters obtained for the two different excess energies. The experimental data do not warrant the evaluation of an inelastic scattering parameter for 9 meV excess energy.

	$\gamma_{\text{tot}}$	$\gamma_{\text{in}}$	$\gamma_{\text{el}}$
9 meV	$8.8 \pm 1.8$	...	$8.8 \pm 1.8$
40 meV	$9.34 \pm 1.53$	$2.54 \pm 0.23$	$6.78 \pm 1.76$

Intriguingly, the total scattering parameters remain remarkably consistent despite the contrasting ionization behaviors exhibited at different excess energies. This suggests that the total interaction strength between excitons

and an electron-hole plasma remains rather unaffected by changes in excess energy. Higher excess energies naturally open pathways for scattering processes involving greater energy transfer. Intuitively, one might anticipate an increase in elastic scattering alongside increased inelastic scattering, as additional scattering possibilities involving a larger energy transfer arise. However, theoretical calculations regarding exciton scattering with electrons in semiconductor quantum wells suggest a preference for small energy-transfer transitions in electron-exciton interactions [15,39,47]. These observations concur with Coulomb scattering of charged particles known from particle physics, which is also more efficient for lower kinetic energies. Accordingly, low-energy, low-momentum electrons scatter far more efficiently elastically with excitons than high-momentum electrons. Although we have no precise knowledge of the energy distribution in our electron-hole plasma, there are comparatively more low-energy electrons for 9 than for 40 meV excess energy excitation.

This corroborates the decrease in the elastic scattering parameter with increased excess energy observed in our experiments. In contrast, inelastic scattering processes show maximum efficiency when the energy transfer between electron and exciton is just large enough to break up the exciton binding energy, as elaborated in Refs. [39,47]. Our experimental results confirm that inelastic scattering becomes more prominent when a significant fraction of the electron-hole plasma possesses sufficient energy to break the exciton bond. Comparing both excess energies, the increase of inelastic scattering processes compensates for the reduced efficiency of elastic scattering, which is also resembled in Table I. This result implies that scattering processes that transfer energies sufficient to break the exciton bond primarily promote the destruction of excitons via inelastic scattering, rather than the increase in their kinetic energy characteristic for elastic scattering processes.

In conclusion, our Letter underscores the pivotal roles of charge carrier excess energies and final state availability in controlling the inelastic scattering behavior of excitons with near-band edge charge carriers. While there is enough excess energy to overcome the exciton binding energy, a lack of final states for the unbound charge carriers prevents the breakup of excitons and allows only elastic scattering. Moreover, we find that the total interaction strength between excitons and an electron-hole plasma remains rather unaltered regardless of the excess energy involved. Intriguingly, increased energy transfer primarily drives the destruction of excitons via inelastic scattering rather than elastic scattering mechanisms that only increase their kinetic energy.

Financial support by the European Regional Development fund through the Innovation Laboratory High-Performance Materials is acknowledged.

\*markus.stein@exp1.physik.uni-giessen.de

- [1] L. Keldysh and A. Kozlov, *Sov. Phys. JETP* **27**, 521 (1968).
- [2] H. Haug and S. Schmitt-Rink, *Prog. Quantum Electron.* **9**, 3 (1984).
- [3] J. Xiang, W. Lu, Y. Hu, Y. Wu, H. Yan, and C. M. Lieber, *Nature (London)* **441**, 489 (2006).
- [4] R. Köhler, A. Tredicucci, F. Beltram, H. E. Beere, E. H. Linfield, A. G. Davies, D. A. Ritchie, R. C. Iotti, and F. Rossi, *Nature (London)* **417**, 156 (2002).
- [5] V. Gantmakher and Y. Levinson, *Carrier Scattering in Metals and Semiconductors* (Elsevier, New York, 2012).
- [6] A. Svizhenko and M. Anantram, *IEEE Trans. Electron Devices* **50**, 1459 (2003).
- [7] Y. Morita, K. Yoshioka, and M. Kuwata-Gonokami, *Nat. Commun.* **13**, 5388 (2022).
- [8] B. Keimer, S. A. Kivelson, M. R. Norman, S. Uchida, and J. Zaanen, *Nature (London)* **518**, 179 (2015).
- [9] O. Schubert, M. Hohenleutner, F. Langer, B. Urbanek, C. Lange, U. Huttner, D. Golde, T. Meier, M. Kira, S. W. Koch *et al.*, *Nat. Photonics* **8**, 119 (2014).
- [10] S. Ito, M. Schüler, M. Meierhofer, S. Schlauderer, J. Freudenstein, J. Reimann, D. Afanasiev, K. Kokh, O. Tereshchenko, J. Güdde *et al.*, *Nature (London)* **616**, 696 (2023).
- [11] A. Honold, L. Schultheis, J. Kuhl, and C. W. Tu, *Phys. Rev. B* **40**, 6442 (1989).
- [12] L. Schultheis, J. Kuhl, A. Honold, and C. W. Tu, *Phys. Rev. Lett.* **57**, 1635 (1986).
- [13] S. Elkomoss and G. Munschy, *J. Phys. Chem. Solids* **38**, 557 (1977).
- [14] S. Elkomoss and G. Munschy, *J. Phys. Chem. Solids* **40**, 431 (1979).
- [15] Y.-P. Feng and H. N. Spector, *J. Phys. Chem. Solids* **48**, 593 (1987).
- [16] B. Deveaud, F. Clérot, N. Roy, K. Satzke, B. Sermage, and D. S. Katzer, *Phys. Rev. Lett.* **67**, 2355 (1991).
- [17] C. Ciuti, V. Savona, C. Piermarocchi, A. Quattropani, and P. Schwendimann, *Phys. Rev. B* **58**, 7926 (1998).
- [18] G. Göger, M. Betz, A. Leitenstorfer, M. Bichler, W. Wegscheider, and G. Abstreiter, *Phys. Rev. Lett.* **84**, 5812 (2000).
- [19] M. Betz, G. Göger, A. Leitenstorfer, M. Bichler, G. Abstreiter, and W. Wegscheider, *Phys. Rev. B* **65**, 085314 (2002).
- [20] T. Yajima and Y. Taira, *J. Phys. Soc. Jpn.* **47**, 1620 (1979).
- [21] L. Schultheis, A. Honold, J. Kuhl, K. Köhler, and C. W. Tu, *Phys. Rev. B* **34**, 9027 (1986).
- [22] M. Fey, M. Stein, C. Fuchs, W. Stolz, K. Volz, and S. Chatterjee, *Phys. Rev. B* **106**, 165303 (2022).
- [23] M. Koch, R. Hellmann, G. Bastian, J. Feldmann, E. O. Göbel, and P. Dawson, *Phys. Rev. B* **51**, 13887 (1995).
- [24] R. Leite, J. Shah, and J. Gordon, *Phys. Rev. Lett.* **23**, 1332 (1969).
- [25] W. Liu, D. Jiang, K. Luo, Y. Zhang, and X. Yang, *Appl. Phys. Lett.* **67**, 679 (1995).
- [26] A. Manassen, E. Cohen, A. Ron, E. Linder, and L. N. Pfeiffer, *Phys. Rev. B* **54**, 10609 (1996).
- [27] H. Wang, K. Ferrio, D. G. Steel, Y. Hu, R. Binder, and S. W. Koch, *Phys. Rev. Lett.* **71**, 1261 (1993).

- [28] D. R. Wake, H. W. Yoon, J. P. Wolfe, and H. Morkoc, *Phys. Rev. B* **46**, 13452 (1992).
- [29] D. Huang, H. Y. Chu, Y. C. Chang, R. Houdré, and H. Morkoc, *Phys. Rev. B* **38**, 1246 (1988).
- [30] S. Chatterjee, C. Ell, S. Mosor, G. Khitrova, H. M. Gibbs, W. Hoyer, M. Kira, S. W. Koch, J. P. Prineas, and H. Stolz, *Phys. Rev. Lett.* **92**, 067402 (2004).
- [31] R. A. Kaindl, M. A. Carnahan, D. Hägele, R. Lövenich, and D. S. Chemla, *Nature (London)* **423**, 734 (2003).
- [32] S. Koch, M. Kira, G. Khitrova, and H. Gibbs, *Nat. Mater.* **5**, 523 (2006).
- [33] M. Stein, F. Schäfer, and L. Gomell, *Phys. Rev. B* **99**, 144310 (2019).
- [34] See Supplemental Material at <http://link.aps.org/supplemental/10.1103/PhysRevLett.132.106901>, which includes Refs. [35–37], for details of the sample, the calculation of the charge carrier densities as well as the Drude-Lorentz analysis and the experimental setup.
- [35] R. Ulbricht, E. Hendry, J. Shan, T. F. Heinz, and M. Bonn, *Rev. Mod. Phys.* **83**, 543 (2011).
- [36] Q. Wu and X. Zhang, *Appl. Phys. Lett.* **67**, 3523 (1995).
- [37] A. Nahata, A. S. Weling, and T. F. Heinz, *Appl. Phys. Lett.* **69**, 2321 (1996).
- [38] P. Steinleitner, P. Merkl, P. Nagler, J. Mornhinweg, C. Schüller, T. Korn, A. Chernikov, and R. Huber, *Nano Lett.* **17**, 1455 (2017).
- [39] G. Ramon, A. Mann, and E. Cohen, *Phys. Rev. B* **67**, 045323 (2003).
- [40] M. Koch, R. Hellmann, G. Bastian, J. Feldmann, E. O. Göbel, and P. Dawson, *Phys. Rev. B* **51**, 13887 (1995).
- [41] A. Manassen, E. Cohen, A. Ron, E. Linder, and L. N. Pfeiffer, *Phys. Rev. B* **54**, 10609 (1996).
- [42] R. C. C. Leite, J. Shah, and J. P. Gordon, *Phys. Rev. Lett.* **23**, 1332 (1969).
- [43] G. Manzke, K. Henneberger, and V. May, *Phys. Status Solidi (b)* **139**, 233 (1987).
- [44] *Ultrafast Phenomena in Semiconductors*, edited by K.-T. Tsen (Springer, New York, New York, NY, 2001).
- [45] A. Efremov, V. Litovchenko, and A. Sarikov, *Mater. Sci. Eng.* **23**, 165 (2003).
- [46] M. Stein, C. Lammers, P.-H. Richter, C. Fuchs, W. Stolz, M. Koch, O. Vänskä, M. J. Weseloh, M. Kira, and S. W. Koch, *Phys. Rev. B* **97**, 125306 (2018).
- [47] J. Choo, Y. Feng, and H. Spector, *J. Phys. Chem. Solids* **55**, 1245 (1994).